JOURNAL OF Materials CHEMISTRY

Interleaved oxovanadium cations in the rancieite manganese oxide δ-MnO_2

Fabrice Leroux,*[a] Annie Le Gal La Salle,[b] Dominique Guyomard[b] and Yves Piffard[b]

[a]*Laboratoire des Matériaux Inorganiques, CNRS-ESA 6002, Université Blaise Pascal, 63177 Aubière cédex, France. E-mail: fleroux@chimtp.univ-bpclermont.fr*
[b]*Institut des Matériaux Jean Rouxel, 2 rue de la Houssinière, BP 32229-44322 Nantes cédex 03, France. E-mail: piffard@cnrs-imn.fr; Fax: 33 2 40 37 39 95; Tel: 33 2 40 37 39 13*

Received 19th September 2000, Accepted 8th November 2000
First published as an Advance Article on the web 4th January 2001

A mixed vanadium manganese oxide was synthesized through a *chimie douce* route. The synthesis proceeds *via* a cationic exchange reaction occurring between the layers of a synthetic rancieite, a lamellar manganic acid. The vanadium atoms were found to be at a distance from Mn close to the Mn–Zn distance in chalcophanite, a model for the phyllomanganates. XAS refinements did not reveal the presence of manganese atoms between the layers of either the protonic or Li-exchanged forms of the rancieite. Li insertion is largely impeded by the presence of dioxovanadium cations, which seem to be accommodated into one of the Li potential sites present in the Li-exchanged phase.

Introduction

In the area of new materials for positive electrodes in lithium batteries, vanadium and manganese oxides appear to be good candidates when considering electrochemical characteristics, such as high average redox potential and reversibility of the lithium insertion process, and for practical attributes, such as low toxicity and cost. Taking into account the different structural forms (*i.e.* the lithium diffusion path), it is well known that Li ions can be readily (de-) inserted between the layers of lamellar structures (2D), as illustrated in the case of deinsertion of lithium ions from host materials such as $LiNiO_2$,[1] $LiCoO_2$[2] and Li insertion into the δ-MnO_2 phases.[3]

However, repetition of the insertion–deinsertion processes may induce the sheets of the host materials to collapse. As a result, the Li ion sites in the electrode materials would be less and less accessible during cycling. Of great importance is the fact that stabilization of the structure may be afforded by small structural modifications, such as migration of cations from the sheets to the interlayer space, as demonstrated by the $Li(Ni,Mg)O_2$ compounds where Mg^{2+} cations migrate between the sheets, thus assuring stability during cycling.[4] To try to avoid such a progressive loss of capacity for δ-MnO_2 rancieite,[5] inorganic complexes were introduced into the interlayer space *via* an exchange reaction. Such "interlayer" pillaring chemistry has been widely exemplified, for instance, through the incorporation of polyoxometallate anions such as $[V_{10}O_{28}]^{6-}$, $[Mo_7O_{24}]^{6-}$ or α-1,2,3$[SiV_3W_9O_{40}]^{7-}$ between the positively charged layers of some lamellar oxyhydroxides[6–8] and through the incorporation of the polyoxocation "Al_{13}" into a buserite, a "10 Å" δ-MnO_2[9] (*i.e.* with an interlayer distance of 10 Å).

In this investigation, we analysed the pillaring reaction of an oxometallate cation of vanadium(v), VO_2^+, when placed between the layers of a "7 Å" δ-MnO_2, the rancieite, and its localisation by the suitable selective X-ray absorption spectroscopy technique (XAS). Using the VO_2^+ interleaved sample for comparison, we discuss the presence or absence of heavy backscattering atoms between the layers of the pristine material, the rancieite in its protonic form, hereafter denoted H-RMO (RMO for rancieite manganese oxide), which is a controversial problem when dealing with phyllomanganates.[10]

Experimental

Sample preparation

The phyllomanganate, rancieite, was prepared by the acid-reducing permanganate salt route.[4] 0.1 dm^3 of concentrated HCl were added to 0.6 dm^3 of 1 M $KMnO_4$ at 60 °C, leading to a precipitate which was left for *ca.* 6 h in the mother liquor. After separation, the precipitate was stirred three times for 4 h with 5 dm^3 of 1 M HNO_3 in 1 dm^3 of distilled water and then washed repeatedly with distilled water, until almost free from the resultant KCl. The synthesis of the Li-exchanged material, denoted Li-RMO, is described elsewhere.[11]

The exchange reaction was performed in an acidic aqueous medium (250 cm^3 of HNO_3: pH *ca.* 0) in which 1 g (9×10^{-3} mol) of rancieite ($MnO_{1.97} \cdot 1.3H_2O$) was dispersed. Since the equilibrium lies in favor of the protons, a large excess of ions is needed to drive the reaction by mass action. An excess of vanadium pentoxide (10 g) was introduced. Under such conditions, V_2O_5 has a solubility of 38.7 g l^{-1} and generates VO_2^+ cations. The solution was sonicated and stirred under reflux conditions at 60 °C. The reaction was repeated three times to complete the exchange. The resulting brown powder was then separated from the solution by centrifugation, washed with deionized water and freeze-dried. This compound is denoted V-RMO.

Physico-chemical analyses

X-Ray diffraction (XRD) patterns were recorded on a Siemens D5000 diffractometer, using Cu-Kα radiation. A Leybold LHS12 ESCA unit was used to record the XPS spectra (XPS mode, focused monochromatized Mg-Kα radiation: 1256.6 eV, residual pressure inside the analysis chamber: $\approx 5 \times 10^{-8}$ Pa). The binding energy was scaled with the 1 s line of carbon (284.6 eV), from the contamination layer. The chemical composition was determined by a combination of analyses; vanadium and manganese contents were determined by atomic emission spectroscopy after dissolution in sulfuric acid and hydrogen peroxide. The active oxygen degree was determined by a potentiometric back titration method.[12] In conjunction with the above, thermogravimetric analysis was carried out on a Perkin-Elmer Model TGS-2 TGA system at a rate of

 DOI: 10.1039/b007596p

10 K min^{-1} from room temperature to 700 °C to obtain the full stoichiometry.

XAS measurements

XAS spectra were performed at LURE (Orsay, France) using X-ray synchrotron radiation emitted by the DCI storage ring (1.85 GeV positrons, average intensity of 250 mA). Data were collected in transmission mode at the manganese K-edge (*ca.* 6539 eV), on the EXAFS III installation, using a double-crystal Si(311) monochromator slighty detuned for harmonic rejection. The EXAFS (extended X-ray absorption fine structure) spectra were recorded from 6430 to 7430 eV with a 2 eV step and two seconds of accumulation time per point. He/Ne-filled ionization chambers were used to measure the incident and the transmitted X-ray flux. Calibration was carried out between all experiments, using a 6 μm Mn foil, by assigning the first point of inflection to the absorption edge. Spectra were recorded at room temperature on samples uniformly dispersed in boron nitride powder and sandwiched between two X-ray transparent Kapton® adhesive tapes.

EXAFS analyses

Experimental data were analyzed following the single scattering theory[13] using the XAS programmes of Michalowicz,[14] as previously described.[15] All the data were of good quality and were analysed without further smoothing or deglitching. The background absorption was calculated using a theoretical expression developed by Lengeler and Eisenberger[16] and the single atomic absorption of the absorber was interpolated by a fourth- or fifth-degree polynomial between 6550 and 7430 eV. Each spectrum was carefully extracted by varying both the degree and first point of the polynomial, and the best removal of low-frequency noise was checked by further Fourier transformation. The energy of the edge, E_0, was taken as being equal to that of the half-height of the absorption. For the $\chi(k)$ simulation, ΔE_0 is a parameter corresponding to a shift of the experimental value of the energy origin, E_0. The normalized EXAFS signal $\chi(E)=[\mu(E)-\mu(E_0]/\mu E_0$ was converted to wave-vector k space, using $k=2m(E-E_0)^{1/2}/h$. The pseudo-radial distribution function (RDF) around the central atom was obtained by a Fourier transform of the weighted $\omega(k)k^3\chi(k)$ spectra, where $\omega(k)$ is a window using a Kaiser function ($\tau=2.5$) defined between 3 and 15 $Å^{-1}$. All the further back-Fourier transforms included a subtraction of this window. Theoretical curves were simulated using the backscattering amplitude and phase shift files of McKale *et al.*[17] The photoelectron mean free path, $\Gamma=k/\lambda(k)$, calculated for an absorber–backscatterer couple was deduced from reference compounds (manganosite MnO and brannerite MnV_2O_6). The overall amplitude scaling factor $S_0{}^2$ was set at 0.66. The refinements were performed by fitting the structural parameters using both simplex and least-squares calculations. These structural parameters are R_i, the distance of the i^{th} shell of the N_i atoms from the absorbing manganese atom, with both thermal and structural disorder expressed through σ_i, the Debye–Waller factor. The energy shift ΔE_0 was also fitted. Previous assumptions indicated that errors can be taken to be 0.003 Å for R_i, 20% for N_i, 0.05 Å for $\Delta\sigma_i$ and 0.3 eV for ΔE_0. The fit residue ρ was calculated following eqn. 1:

$$\rho=\frac{\sum_k k[k\chi_{exp}(k)-k\chi_{calc}(k)]^2}{\sum_k k[k\chi_{exp}(k)]^2} \quad (1)$$

Battery preparation and testing

Prior to electrochemical testing, the samples were heated at 180 °C to avoid the presence of hydration water. The active material was then mixed with carbon black (Super S from Chemetals Inc., Baltimore, MD, USA), 9 wt%, and PVDF binder, 4 wt%, to make a composite electrode on an aluminium disk. Electrodes had surface areas of 1 cm^2 and contained about 5 mg of active material. The electrolyte was a 1 M solution of $LiClO_4$ in a 2:1 (v/v) mixture of EC and DMC. Swagelok test cells were assembled in an argon-filled glove box with moisture and oxygen levels of less than 1 ppm. Li metal was used as the anode. The batteries were tested using a Mac-Pile system (Claix, France) in galvanostatic mode. Different current densities were used, corresponding to different discharge rates, denoted *C/n* (discharge time of *n* hours). Li insertion per unit formula weight was calculated from the elapsed time and the mass of active material according to Faraday's law.

Results and discussion

1 Stoichiometry of the V-oxometallate interleaved rancieite material

The inorganic manganic acid prepared in this work belongs to the rancieite family. As a result of the work of Richmond *et al.*,[18] rancieite is considered an independent species, along with the other "7 Å" δ-MnO_2 materials and the birnessite group.[19] The structure consists of layers of edge-sharing MnO_6 octahedra arranged in a CdI_2-type structure and interleaved with water molecules and protons. The average Mn–O distance is 1.89 Å, in agreement with an Mn oxidation state of *ca.* 4+ based on empirical bond valence sum calculations.[20] The crystallinity of the material is rather poor and, accordingly, only weak (00*l*) peaks are observed on the XRD pattern; they correspond to an interlayer distance of 7.4 Å.

For the V-RMO material, only the ill-defined (00*l*) first harmonic is observed, suggesting a small number of stacked layers. This is often the case after exchange reactions, although the interlayer distance remained unchanged. The ratio of vanadium per manganese atom was found to be 0.11. This corresponds to an exchange rate of only 16.4% if one considers a theoretical exchange capacity of 7.22 meq g^{-1} [4] or of 26.2% if one takes into account the apparent Li^+ exchange capacity determined previously.[10] Such a low exchange rate can be explained by the low pH, required for the presence of the cationic $VO_2{}^+$ species,[21] which does not favor the removal of protons from the rancieite.

Before considering further characterization, it is vital to know whether the exchange reaction really occurred between the layers of the rancieite. To answer the question of whether or not the vanadium ions are located in a specific site between the layers or adsorbed onto the material surface and to clarify a lack of structural information, XAS experiments were carried out at the manganese K-edge.

2 Localization of the vanadium atoms

For comparison, moduli of the Fourier transforms of the experimental EXAFS data are presented for the pristine material, and the Li-exchanged and V-exchanged phases in Fig. 1. All three pseudo-radial distribution functions (RDF) exhibit two well-defined peaks that correspond to the first shell of oxygen neighbors and the first shell of manganese neighbors around the manganese atoms. From the similarity in their features, the local environments of the manganese atoms are nearly identical in these three samples. The results of the refinements are given in Table 1. It is noteworthy that all the parameters were free to move during the refinement. Shell contributions were isolated from each other after Fourier filtering, except in the case of the V-exchanged sample for which it was not possible to disentangle the two peaks, ⟨Mn–Mn⟩ and ⟨Mn–V⟩ (*vide infra*). The immediate surroundings of manganese atoms in the three samples (approximately six

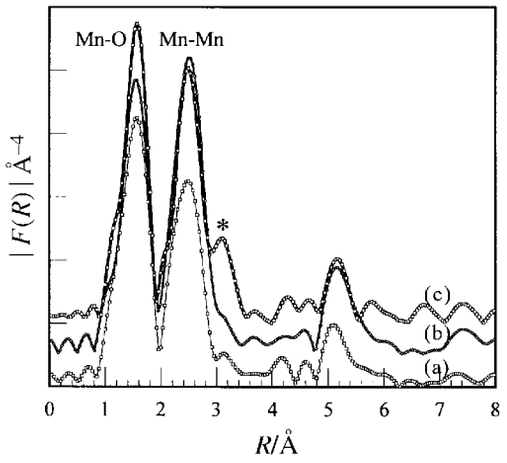

Fig. 1 Moduli of the Fourier-transformed experimental EXAFS data (Mn K-edge) for (a) H-RMO, (b) Li-RMO and (c) V-RMO. Note that, in the absence of a phase correction, the peaks are displaced to lower values than the structural values (Table 1).

oxygen atoms at the same distance of *ca.* 1.9 Å) indicate the presence of MnO_6 octahedra: the $\langle$Mn–O$\rangle$ bond lengths are consistent with manganese oxidation states of *ca.* +4. The values of the Debye–Waller factor, $\Delta\sigma \approx 5.10^{-2}$ Å, can be interpreted in terms of a rigid sub-lattice of the first oxygen shell which surrounds the manganese atoms. The second shell, arising from the nearest manganese atoms, is found at a distance of 2.86 Å. This value is consistent with the presence of edge-sharing MnO_6 octahedra.[22]

In the case of the V-exchanged sample, a third contribution is clearly observed on the RDF (marked with an asterisk in Fig. 1). The inverse Fourier transform isolated to the $\langle$Mn–X$\rangle$ contribution, shows a gradual decrease in amplitude of the sinusoidal oscillations; this can be explained only by the presence of heavy backscattering atoms (not oxygen atoms) surrounding the manganese atoms. As no such contribution is observed for the pristine material or for the Li-exchanged material, the peak was attributed to the presence of vanadium atoms. The refinement is shown in Fig. 2 and the result of the fitting procedure is presented in Table 1. The interatomic distance $\langle$Mn–V$\rangle$ (3.44 Å) is very close to that observed for $\langle$Mn–Zn$\rangle$ (3.49 Å) in the chalcophanite, $ZnMn_3O_7{\cdot}3H_2O$ (structural model for the phyllomanganates).[23]

The above facts led us to surmise that the vanadium atoms were introduced between the layers of the rancieite during the exchange reaction, contradicting the hypothesis that the vanadium atoms were present as an impurity. This result supports the ability of the phyllomanganate structure to accommodate large interlayer cations, as confirmed by other authors.[9] In contrast, however, the interlayer space for the pristine material and for the Li-exchanged sample was found to be free from heavy backscattering ions, *i.e.* Mn^{3+}. The presence of such ions has been suggested for birnessite.[9] This

Table 1 Results of the fits for the EXAFS analysis at the Mn K-edge for V-RMO

Sample	Shell	*R*/Å	*N*	$\Delta\sigma^2$/Å^2	ρ (%)
H-RMO	Mn–O	1.89	5.9	0.0016	2
	Mn–Mn	2.86	4.3	0.0059	5
Li-RMO	Mn–O	1.90	5.6	0.0025	1
	Mn–Mn	2.86	4.5	0.0049	6
	Mn–O	1.92	5.5	0.0023	2
V-RMO	Mn–Mn	2.87	4.5	0.0042	0.7
	Mn–V[a]	3.44	1.0	0.0053	

[a]The nature of the backscattering atom is given by comparison to the RDFs (see text).

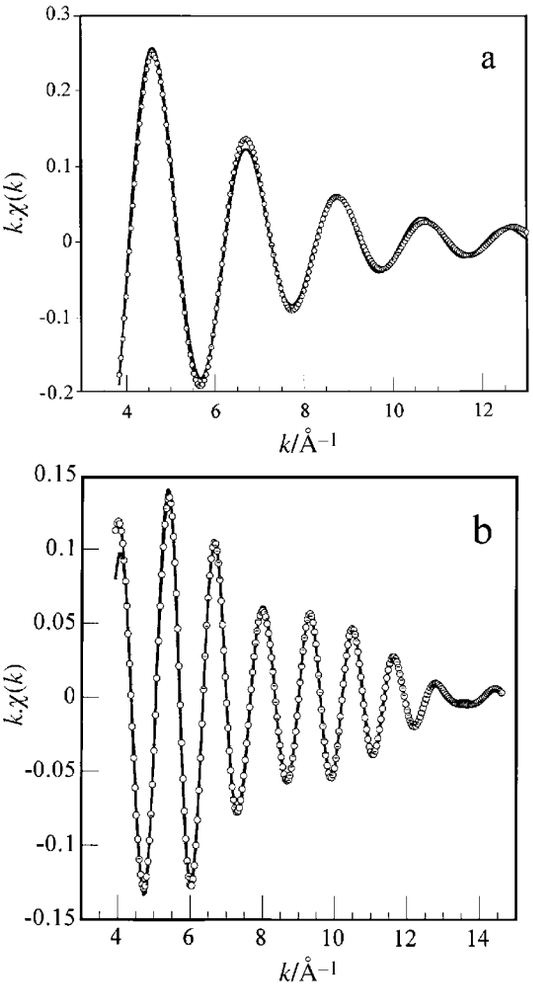

Fig. 2 Experimental (···) and simulated (—) EXAFS (k^3 weighted) oscillations of V-RMO. (a) Oscillations for the first shell surrounding the manganese atoms (oxygen) and (b) oscillations corresponding to the presence of the two immediate metal–metal distances, Mn–Mn and Mn–V (see text).

is an important observation that, together with other comparisons,[10] underlines the difference between the rancieite and birnessite-type compounds. It should be noted that, in spite of its quasi-amorphous nature, the V-RMO material presents a well-defined local order, related to the pristine material. The metal second shell is also observed on the RDFs. As shown by the example of Zn-substituted nickel hydroxides,[24] XAS is an appropriate technique for addressing the issue of the location of interleaved species in lamellar materials.

3 Chemical formula

Chemical analysis of the oxidation state of Mn in the V-exchanged sample was carried out according to a method developed by Vetter and Jaeger.[12] No change in the oxidation state was observed before and after the exchange reaction. The oxidation states of the transition metals were determined by XPS (not shown). The 2p energy levels were consistent with an oxidation state of +5 for vanadium[25] [$E(2p_{3/2}) = 516.4$ eV] and +4 for manganese [$E(2p_{3/2}) = 642.1$ eV].

The thermal behavior of V-RMO is shown in Fig. 3. As for the pristine material,[10] the TG curve shows a fairly rapid weight loss up to 150 °C, followed by a smooth slope up to 550 °C. The XRD pattern of the powder obtained following thermogravimetric analysis (heat treatment to 700 °C) provides identification of two phases, Mn_3O_4 hausmannite and

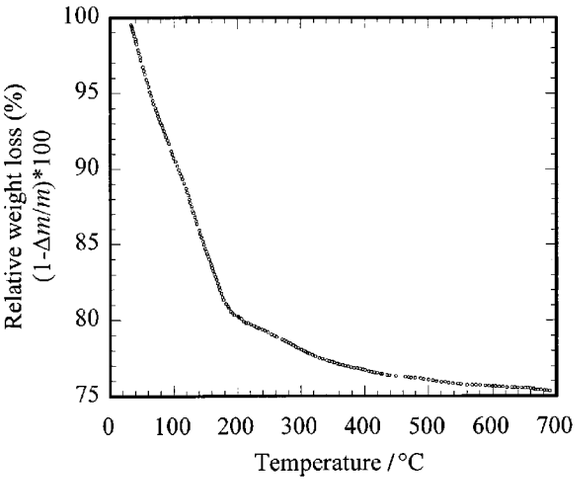

Fig. 3 TG curve of the V-RMO sample.

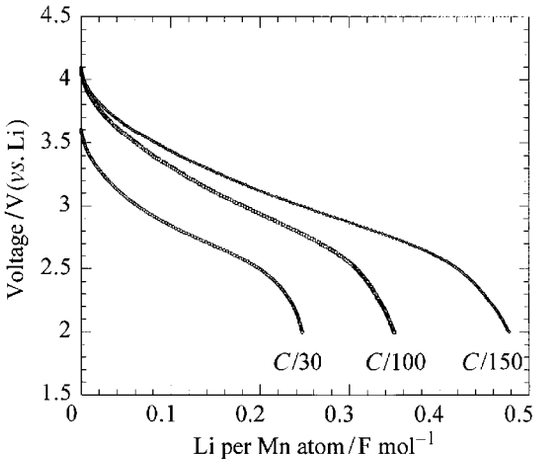

Fig. 4 Voltage–composition curves for V-RMO at the three first discharges in the 4.3–2.0 V range. The first, second and third discharges were performed at current densities corresponding to rates of *C*/30, *C*/100 and *C*/150, respectively.

MnV_2O_6. Therefore the decomposition reaction can be written as shown in eqn. 2:

$$(V_zMn)O_y{\cdot}nH_2O \rightarrow z/2MnV_2O_6 + 1/3(1-z/2)Mn_3O_4 + 1/2(y-7z/3-4/3)O_2 + nH_2O \quad (2)$$

The first process mostly involves the departure of hydration water, whereas the second corresponds to the oxygen loss giving rise to the reduced Mn oxide and MnV_2O_6. As *n* and *z* are known separately, the chemical formula can be written as $(V_{0.11}Mn)O_{2.24}{\cdot}0.8H_2O$, or as $[(VO_2)^+_{0.11}H^+_{0.39}{\cdot}0.6H_2O]_{inter}(MnO_{2.21})_{intra}$ if one wants to refer to the intralamellar composition and the interlayer domain. The chemical formulae of the pristine material, and the Li-RMO and V-RMO phases at room temperature and after treatment at 180 °C are listed in Table 2.

4 Electrochemistry

The Li intercalation behavior of V-RMO, measured at decreasing current densities for successive discharge–charge cycles, is reported in Fig. 4. The lowest current density (corresponding to a rate of *C*/150) may be taken as a quasi-equilibrium condition. *V versus x* discharge curves show a rough S-shape and not a plateau, which seems to indicate a topotactic single phase transformation, as expected for the Li insertion process for a 2D system.

Comparison of the Li insertion capacities clearly shows two main points: (i) Li intercalation into V-RMO is a slow kinetic process, and (ii) Li uptake in V-RMO is lower than in Li-RMO[3c]

This diffusion limitation may arise from spatial hindrance, since there is no electronic limitation. This could be explained by the presence of repulsive VO_2^+ cations between the layers. Comparison of the electronic density curve to that of the pristine material will shed some light on the lowering of the Li uptake. The d*x*/d*V versus V* curve is calculated from the first discharge of Fig. 4. A corresponding curve for Li-RMO, obtained under similar experimental conditions, is also displayed for comparison (Fig. 5). It is noteworthy that these curves do not provide truly thermodynamic data. For Li-RMO, two Li potential sites are observed, at 2.7 and 2.95 V *vs.* Li, whereas only one site, at 2.7 V *vs.* Li, can be seen for V-RMO. This comparison prompts us to surmise that the interleaved dioxovanadium cations may occupy the Li potential site at 2.95 V (S_1), leaving only the site at lower potential available for Li insertion. The difference in area under the curves (Fig. 5) demonstrates the lower Li uptake for V-

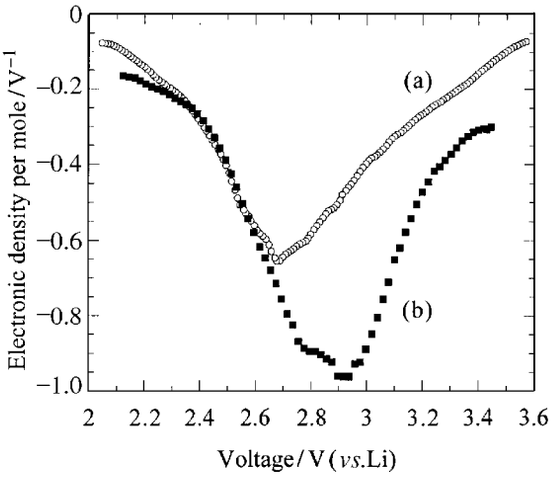

Fig. 5 Electronic density curve *vs. V* for the first discharge (in quasi-equilibrium condition) of (a) V-RMO and (b) Li-RMO.

Table 2 Compositions of the samples at room temperature and after thermal treatment at 180 °C

Sample	Mean oxidation state of Mn	Chemical formula[a]	Reference
H-RMO			
rt	3.94	$Mn^{III}_{0.06}Mn^{IV}_{0.94}O_{1.97}{\cdot}1.3H_2O$	10
180 °C	3.72	$Mn^{III}_{0.28}Mn^{IV}_{0.72}O_{1.86}{\cdot}\varepsilon H_2O$	10
Li-RMO			
rt	3.94	$Li_{0.42}Mn^{III}_{0.06}Mn^{IV}_{0.94}O_{2.18}{\cdot}1.41H_2O$	10
180 °C	3.88	$Li_{0.42}Mn^{III}_{0.12}Mn^{IV}_{0.88}O_{2.15}{\cdot}\varepsilon H_2O$	10
V-RMO			
rt	3.94	$V^{V}_{0.11}Mn^{III}_{0.06}Mn^{IV}_{0.94}O_{2.24}{\cdot}0.8H_2O$	This work
180 °C	3.86	$V^{V}_{0.11}Mn^{III}_{0.14}Mn^{IV}_{0.86}O_{2.20}{\cdot}\varepsilon H_2O$	This work

[a]The chemical formulae are expressed by manganese atom.

RMO, as this area is directly related to the number of inserted Li ions.

Conclusions

The rancieite-type layered proton-containing manganese oxide (H-RMO) is a manganic acid that behaves as an ion exchanger. By taking advantage of these ion exchange properties, a VO_2^+ derivative has been prepared in an acidic medium; its chemical formula corresponds to $(V_{0.11}Mn)O_{2.24}{\cdot}0.8H_2O$. Structural studies of this compound through the use of XAS have shown that the V species lie within the interlayer space of V-RMO. In contrast, this interlayer domain was found to be free of Mn species in the pristine material, thus underlining the difference between the rancieite and the birnessite-type compounds. From an electrochemical point of view, the presence of dioxovanadium cations is a hindrance to the Li insertion process, as illustrated by the loss of the Li site at higher potential, which explains the decreased Li insertion capacity of V-RMO compared to the pristine material.

References

1 J. R. Dahn, U. von Sacken, M. W. Juzkow and H. Al-Janaby, *J. Electrochem. Soc.*, 1991, **138**, 2207.
2 K. Sekai, H. Azuma, A. Omaru, S. Jujita, H. Imoto, K. Yamaura, Y. Nishi, S. Mashiko and M. Yokogawa, *J. Power Sources*, 1993, **43–44**, 241.
3 (*a*) R. Chen, T. Chirayil, P. Zavalij and M. S. Whittingham, *Solid State Ionics*, 1996, **86–88**, 1; (*b*) S. Bach, J. P. Pereira-Ramos and N. Baffier, *J. Electrochem. Soc.*, 1996, **143**, 3429; (*c*) F. Leroux, D. Guyomard and Y. Piffard, *Solid State Ionics*, 1995, **80**, 307.
4 C. Pouillerie, L. Croguennec, Ph. Biensan, P. Willmann and C. Delmas, *Abstracts of the 10th International Meeting on Li batteries, Come, Italy, May 2000*, The Electrochemical Society, USA, 2000, abstract 237.
5 M. Tsuji, S. Komarni, Y. Tamaura and M. Abe, *Mater. Res. Bull.*, 1992, **27**, 741.
6 C. Depège, L. Bigey, C. Forano, A. de Roy and J. P. Besse, *J. Solid State Chem.*, 1996, **126**, 314.
7 M. A. Drezdon, *Inorg. Chem.*, 1988, **27**, 4628.
8 E. Narita, P. D. Kaviratna and T. J. Pinnavaia, *J. Chem. Soc., Chem. Commun.*, 1993, 60.
9 S. Wong and S. Cheng, *Inorg. Chem.*, 1992, **31**, 1165.
10 P. Strobel, J. Durr, M. Tuillier and J. C. Charenton, *J. Mater. Chem.*, 1993, **3**, 453.
11 F. Leroux, D. Guyomard and Y. Piffard, *Solid State Ionics*, 1995, **80**, 299.
12 K. J. Vetter and N. Jaeger, *Electrochim. Acta*, 1966, **11**, 401.
13 B. K. Teo, *EXAFS: Basic Principles and Analysis*, Springer-Verlag, Berlin, 1986.
14 A. Michalowicz, in *Logiciels pour la Chimie*, Société Française de Chimie, Paris, 1991.
15 F. Leroux, Y. Piffard, G. Ouvrard, J.-L. Mansot and D. Guyomard, *Chem. Mater.*, 1999, **11**, 2948.
16 B. Lengeler and P. Eisenberger, *Phys. Rev. B*, 1980, **21**, 4507.
17 A. G. Mc Kale, B. W. Veal, A. P. Paulikas, S. K. Chan and G. S. Knapp, *J. Am. Chem. Soc.*, 1988, **110**, 3763.
18 W. E. Richmond, M. Fleisher and M. Rose, *Bull. Soc. Fr. Mineral. Cristallogr.*, 1969, **92**, 191.
19 R. Giovanoli, E. Stähli and W. Feitknecht, *Helv. Chim. Acta*, 1970, **53**, 453.
20 I. D. Brown and R. D. Shannon, *Acta Crystallogr., Sect. A*, 1973, **29**, 266.
21 E. Deltombe, N. de Zoubov and M. Pourbaix, *Rapport technique du CEBELCOR*, Gauthier-Villars and Cie, Paris, 1963.
22 A. Manceau, *Am. Mineral.*, 1989, **74**, 1386.
23 A. D. Wadsley, *Acta Crystallogr.*, 1955, **8**, 165.
24 C. Tessier, L. Guerlou-Demourgues, C. Faure, A. Demourgues and C. Delmas, *J. Mater. Chem.*, 2000, **10**, 1185.
25 C. D. Wagner, W. M. Riggs, L. E. Davis, J. F. Moulder and G. E. Muilenberg, *Handbook of X-Ray Photoelectron Spectroscopy*, Perkin-Elmer Corporation, Eden Prairie, USA, 1979.